

# Inverse-square law between time and amplitude for crossing tipping thresholds

Paul Ritchie\*

*Earth System Science, College of Life and Environmental Sciences,  
Harrison Building, University of Exeter, Exeter, EX4 4QF, United Kingdom*

Özkan Karabacak†

*Centre for Systems, Dynamics and Control, College of Engineering,  
Mathematics and Physical Sciences, Harrison Building,  
University of Exeter, Exeter, EX4 4QF, United Kingdom and  
Department of Electronics and Communication Engineering,  
Istanbul Technical University, 34469 Istanbul, Turkey*

Jan Sieber‡

*Centre for Systems, Dynamics and Control, College of Engineering,  
Mathematics and Physical Sciences, Harrison Building,  
University of Exeter, Exeter, EX4 4QF, United Kingdom*

(Dated: June 2, 2022)

A classical scenario for tipping is that a dynamical system experiences a slow parameter drift across a fold (usually caused by a run-away positive feedback loop). We study how rapidly one needs to turn around once one has crossed the threshold. We derive a simple criterion that relates the peak and curvature of the parameter path in an inverse-square law to easily observable properties of the dynamical system near the fold.

For the case when the dynamical system is subject to stochastic forcing we give an approximation to the probability of tipping for parameter paths that are turning around near the tipping point.

In mathematical terms our scenario is a non-transversal encounter of a fold bifurcation (in contrast to a transversal crossing).

The derived approximations are valid if the parameter path is traversed sufficiently slowly. We demonstrate for a higher dimensional system how numerically observed escape from the equilibrium converge to our asymptotic expressions. The inverse-square law between peak and curvature of the parameter path is also visible in the level curves of equal probability when the system is subject to random disturbances.

A common scenario in nonlinear systems is that they possess thresholds in parameter space (so-called bifurcations) where their steady-state behaviour changes qualitatively. For example, in simple models of the Indian Summer Monsoon, increasing the planetary albedo  $A$  (reflection of incoming sun-light due to whiteness of the surface), causes the Summer Monsoon to shut down. The underlying mechanism is a run-away positive feedback effect between moisture advection and the temperature difference between the land and ocean. In the mathematical model this effect creates a fold of steady states: a stable steady state of the system disappears at some critical value of the albedo  $A^b$  (the *tipping point*) in a fold (becoming unstable).

When the albedo  $A$  changes over time, increasing beyond the tipping threshold  $A^b$ , the monsoon will shut down. This shutdown is slightly delayed compared to the crossing, if

the change of albedo is relatively fast, giving time to avoid tipping when the albedo change is reversed. The relation between the time  $t$  which the albedo may spend above the level  $A^b$  and the maximal amount  $q = \max_t(A(t)) - A^b$  by which the albedo may exceed the level  $A^b$  follows an inverse-square law: if  $q \times t^2$  is less than a critical level  $16/d$  then tipping is avoided, when it is larger than  $16/d$ , tipping occurs. The level  $d$  is the derivative with respect to the parameter of the square of the decay rate toward stable equilibria near the fold. The quantity  $d$  can thus be estimated from the autocorrelation in time series of system outputs. The inverse-square relation holds approximately for all cases of tipping caused by positive feedback (folds).

If the system is subject to random disturbances the level curves of equal probability (for example, the set of exceedance times  $t$  and exceedance amplitudes  $q$  where tipping probability is 50%) also follow similar inverse-square laws approximately. We provide a few general approximation formulas for these probabilities and test them on the In-

\* Paul.Ritchie@exeter.ac.uk

† O.Karabacak@exeter.ac.uk

‡ J.Sieber@exeter.ac.uk

dian Summer Monsoon model.

## I. INTRODUCTION

The phenomenon of tipping is subject to ongoing intense study within the scientific community due to its prominence in complex systems, including climate [1–4], ecosystems [5–8] and finance [9]. The notion of tipping usually refers to a sudden large qualitative change in output behaviour caused by a small change to input levels or rates [10]. The classical and most common model case for tipping is that the system can be described (possibly at a coarse level) as a dynamical system with a slowly drifting system parameter which passes slowly through a fold (or saddle-node) bifurcation. In scientific terms the mathematical scenario of a fold bifurcation at some system parameter value corresponds to the presence of internal positive feedback loops, which, with sufficient internal amplification, lead to a run-away scenario.

In Section III we will introduce a simple Indian Summer Monsoon model, originally derived by Zickfeld [11], which we will use for illustration throughout. In this model a positive feedback loop is formed between the temperature difference over the Indian Ocean and Indian subcontinent and moisture advection [12]. In the summer months the temperature over land warms quicker than the temperature over the ocean, which creates winds coming off the ocean onto land [11]. The winds carry moisture which is deposited over the land in the form of precipitation. This process releases latent heat, causing the temperature over land to increase, creating a greater temperature difference and thus generating stronger winds to complete the positive feedback loop. Zickfeld *et al.* [13] identified a tipping threshold in the planetary albedo, such that increasing the albedo above this value will cause the monsoon to shutdown.

The classical tipping scenario considers a gradual parameter change that varies the system parameter slowly through the tipping threshold (the fold bifurcation parameter value), causing a transition from the current gradually varying equilibrium to a new state, possibly far away in state space. However, we may expect that this transition is delayed with respect to the passage through the tipping threshold if the system is forced at a faster than infinitesimal speed [14, 15]. This delay may pose policy relevant questions, since many real life scenarios, particularly in climate [16], display similar characteristics to those of a fold bifurcation transgression. For example, the Atlantic Meridional Overturning Circulation (AMOC) can be disrupted or even stopped by an increase of freshwater to the North Atlantic [17]. However, due to the slow response time of the system [18, 19] it may be possible to exceed the critical threshold for some time but still maintain the circulation if the freshwater forcing is reduced to values below a critical level sufficiently rapidly.

We will investigate this for the example model of the

Indian Summer Monsoon, one of the policy relevant tipping elements in the climate system identified by Lenton *et al.* [1]. For this climate subsystem, policy makers may be interested in understanding: if the albedo was increased beyond the threshold, can the albedo be reversed quickly enough to prevent a shutdown of the monsoon? We illustrate the inverse square law for the maximal permitted exceedance value and time over the tipping threshold in Zickfeld’s model.

*General deterministic result* (see Section II) Let us assume that a system governed by differential equations has a fold in system parameter  $q$  at value  $q^b$  and that the stable equilibrium involved in the fold exists for  $q < q^b$ . We assume that the parameter  $q = q(\epsilon t, \epsilon)$  changes slowly in time (with speed  $\epsilon$ ), reaches a maximum near the tipping point at a value  $q^{\max} > q^b$  ( $q^{\max} - q^b \sim \epsilon$ ), and spends time  $t_e \sim \epsilon^{-1/2}$  (called the *exceedance time*) above the critical level  $q^b$ . Then the inverse square law contains only one system specific proportionality factor  $d$ , which is independent of the parameter path. Tipping is avoided if

$$\underbrace{\left[ \frac{\partial}{\partial q} [(-\lambda(q))^2] \Big|_{q=q^b} \right]}_d (q^{\max} - q^b) t_e^2 \leq 16. \quad (1)$$

In this expression  $\lambda(q)$  is the leading eigenvalue of the linearization of the system at the stable equilibrium, which is zero for  $q = q^b$ . The inequality given by (1) is valid and a sharp boundary for sufficiently small  $\epsilon$ .

In real-world applications there is often no direct access to an underlying model. Instead, only time series output data, disturbed by random fluctuations, may be available, such as proxies for the temperature and  $CO_2$  [20] in palaeo-climate records. One may estimate the quantity  $d$  from the time- $\Delta t$  autocorrelation  $a(q)$  of a times series with approximately stationary parameter  $q$  close to the critical value  $q^b$  via

$$d \approx \frac{(1 - a(q))^2}{(\Delta t)^2 (q - q^b)} \quad \text{for } q < q^b, q \approx q^b.$$

The autocorrelation and variance of output time series are expected to increase when the parameter approaches  $q^b$  from below, if the time dependence of the parameter path is sufficiently small ( $\epsilon \ll 1$ ). This has motivated extensive studies in field data (such as palaeo climate records or lake sediments), investigating whether autocorrelation and variance act as *early-warning indicators* of tipping [16, 21–23]. See also Ritchie and Sieber [24] for a study on the behaviour of early-warning indicators when the parameter is changed at higher speed, causing rate-induced tipping.

*Probabilistic result* (see Section IV) If the system is subject to small random white-noise disturbances, tipping may occur with positive probability even if the parameter path never exceeds  $q^b$ . Thus, the exceedance time  $t_e(q_0)$ , measuring the time the parameter path  $q(\epsilon t, \epsilon)$  spends above a fixed parameter value  $q_0 < q^b$

becomes a relevant parameter. We denote by  $2D$  the variance of the random disturbances per time step, projected onto the critical direction (the eigenvector for the eigenvalue  $\lambda(q^b) = 0$  of the linearization of the system at parameter  $q^b$ ).

In these parameters we find that the level curves of constant probability of tipping follow the inverse square law approximately if  $\epsilon \sim D^{2/3}$  and, hence,  $q^{\max} - q^b \sim D^{2/3}$  and  $t_e(q_0) \sim D^{-1/3}$ . If  $\epsilon \gg D^{2/3}$ , the probabilistic result reverts to the deterministic case, while for  $\epsilon \ll D^{2/3}$  the tipping probability is close to 1. We provide a numerically computed graph of escape probabilities that is accurate in the limit  $\epsilon \rightarrow 0$  and  $D^{2/3} \sim \epsilon$ . We also provide approximations for the escape probabilities in several limiting cases of the provided graph.

In Section V we will illustrate the escape probability estimates for the monsoon model with additive noise. After the summary in Section VI, appendices will give detailed expressions for the projection of the  $n$ -dimensional system onto a scalar ODE, and for the approximations of the escape probability in the presence of noise.

## II. CRITICAL DISTANCE AND TIME OVER THRESHOLD BEFORE TIPPING

We consider an  $n$ -dimensional system of ordinary differential equations (ODEs) with a scalar output  $y_o$

$$\begin{aligned}\dot{\mathbf{y}}(t) &= f(\mathbf{y}(t), q), \quad \mathbf{y}(t) \in \mathbb{R}^n, q \in \mathbb{R} \\ y_o(t) &= \mathbf{w}^T \mathbf{y}(t), \quad y_o(t) \in \mathbb{R}, \mathbf{w} \in \mathbb{R}^n.\end{aligned}\quad (2)$$

that has a fold (saddle-node) bifurcation at  $(\mathbf{y}, q) = (\mathbf{y}^b, q^b)$ . Specifically, we make the following assumptions ((S1)-(S4) define the fold bifurcation [25]):

- (S1) the linearization  $A_1 = \partial_1 f(\mathbf{y}^b, q^b)$  is singular and has a single right nullvector  $\mathbf{v}_0$  and a single left nullvector  $\mathbf{w}_0$  ( $A_1 \mathbf{v}_0 = 0$ ,  $\mathbf{w}_0^T A_1 = 0$ ), scaled such that  $\mathbf{w}_0^T \mathbf{v}_0 = 1$ ;
- (S2) all other eigenvalues of  $A_1$  have negative real part: one of the branches of the fold is stable;
- (S3)  $a_0 := \mathbf{w}_0^T \partial_2 f(\mathbf{y}^b, q^b) \neq 0$ : changing the parameter  $q$  crosses the fold transversally;
- (S4)  $\kappa := \frac{1}{2a_0} \mathbf{w}_0^T \partial_1^2 f(\mathbf{y}^b, q^b) \mathbf{v}_0^2 \neq 0$ : only one node and one saddle collide in the fold;
- (S5)  $\mathbf{w}^T \mathbf{v}_0 \neq 0$ : one can observe the dynamics in the critical direction  $\mathbf{v}_0$  through the output  $y_o$ ; thus we scale  $\mathbf{v}_0$  such that  $\mathbf{w}^T \mathbf{v}_0 = 1$ .

Without loss of generality we assume that the stable equilibrium involved in the fold exists for  $q < q^b$  and the stable equilibria have output  $y_o < y_o^b := \mathbf{w}^T \mathbf{y}^b$ , such that the signs of  $a_0$  and  $\kappa$  are positive:

$$a_0 > 0, \quad \kappa > 0.$$

Otherwise, we may change the sign of the considered output projection  $\mathbf{w}$  or parameter  $q$ .

This section will study the question how this bifurcation effectively changes when the parameter  $q$  varies

slowly in time along a path of the form  $q(\epsilon t, \epsilon)$  with a small  $\epsilon$ .

For the function  $q(\epsilon t, \epsilon)$  we assume the following about the path:

- (P1)  $q(0, 0) = q^b$ : the parameter reaches the fold bifurcation value (without loss of generality) at time 0;
- (P2)  $\partial_1 q(0, 0) = 0$ : the encounter of the fold is *non-transversal* (we may shift time such that  $\partial_1 q(0, \epsilon) = 0$  also for  $\epsilon \neq 0$ );
- (P3)  $\partial_1^2 q(0, 0) < 0$ : the parameter path  $q(\epsilon t, \epsilon)$  has a maximum at time  $t = 0$ .

Assumption P2 implies that we are studying the vicinity of a degeneracy. Commonly, one assumes that the crossing of the bifurcation is transversal (that is,  $\partial_1 q(0, 0) > 0$ , making P3 unnecessary)[26–30]. This is called a slow (in comparison to the response time of the system) passage through a fold bifurcation. For the transversal case it has been shown [14, 15] that solutions track the stable equilibrium branch for  $t < 0$  at a distance of order  $\epsilon^{1/3}$  and that solutions gain distance of order 1 from the equilibrium branch with a delay of order  $\epsilon^{2/3}$  such that  $y(t) - y^b \sim O(1)$  for times  $t \sim \epsilon^{2/3}$ . The textbook by Berglund and Gentz[14] also derives asymptotic probabilities and escape times for tipping in the presence of white noise in the small- $\epsilon$ -small-variance regime.

Throughout our paper we assume that the parameter  $\epsilon$  is small, making the system (2) with parameter  $q(\epsilon t, \epsilon)$  a slow-fast system. When we expand the path  $q(\epsilon t, \epsilon)$  with respect to time  $t$  we are justified in dropping higher-order derivatives of the path as they are scaled with higher powers of  $\epsilon$ .

The assumptions imply that we have for fixed  $q < q^b$  a branch of stable equilibria  $(\mathbf{y}^s(q), q)$  and a branch of unstable equilibria  $\mathbf{y}^u(q)$  of (2) (all satisfying  $0 = f(\mathbf{y}^{s,u}(q), q)$ ), which meet in the fold at parameter  $q^b$  in point  $\mathbf{y}^b$ . We expect a solution  $\mathbf{y}(t)$ , starting from close to  $\mathbf{y}^s(q(\epsilon t_0, \epsilon))$  with  $t_0 < 0$  to follow the stable branch closely for sufficiently small  $\epsilon$  until we reach the vicinity of  $\mathbf{y}^b$  at time  $t$  close to 0.

In the vicinity of the fold  $(\mathbf{y}^b, q^b)$ , we may zoom in and speed up time:

$$\begin{aligned}x &:= \epsilon^{-1/2} (y_o - y_o^b) = \epsilon^{-1/2} \mathbf{w}^T (\mathbf{y} - \mathbf{y}^b), \\ t_{\text{new}} &:= \epsilon^{1/2} t_{\text{old}}.\end{aligned}\quad (3)$$

Then  $x$  satisfies the scalar differential equation

$$\begin{aligned}\dot{x} &= a_0 (R_0 - R_2 t^2 + \kappa x^2) + O(\epsilon^{1/2}), \quad \text{where} \\ R_0 &:= \partial_2 q(0, 0), \quad R_2 := -\partial_1^2 q(0, 0) > 0\end{aligned}\quad (4)$$

It is clear that, if  $R_0$  is sufficiently large, the trajectory  $x(t)$  will grow to large values. Thus,  $\mathbf{y}(t)$  will leave the neighborhood of the branches of equilibria (corresponding to tipping).

The quantities  $a_0$  and  $\kappa$  can be estimated from observations of the output  $x$  for fixed parameter  $q, q^b$  (thus,  $R_2 = 0$ ):  $2\kappa$  is the curvature of the equilibrium curve as observed through  $x$  in  $x = 0$ , and the decay rate for parameter values equal to  $R_0$  (for  $R_2 = 0$ ) toward the stable

equilibrium for  $R_0\kappa < 0$  equals  $-2a_0\sqrt{-R_0\kappa}$ . Note that this is the decay rate for the sped up time  $t_{\text{new}}$ .

In the limit  $\epsilon = 0$ , the scalar equation (4) has solutions that are asymptotically  $x(t) \sim -|t|\sqrt{R_2/\kappa}$  for large  $t$  if

$$R_0 < \frac{1}{a_0} \sqrt{\frac{R_2}{\kappa}}. \quad (5)$$

The limiting orbit of (4), for  $\kappa a_0^2 R_0^2 = R_2$  and  $\epsilon = 0$ , is  $x(t) = t\sqrt{R_2/\kappa}$ . In the original coordinates, this gives a first-order expansion for the condition relating the maximum value of  $q$  (which it attains at  $t = 0$ :  $q(0, \epsilon) = \max_t q(\epsilon t, \epsilon)$ ) and its second time derivative  $\ddot{q}(0, \epsilon) = \frac{d^2}{dt^2}q(\epsilon t, \epsilon)|_{t=0}$  to each other. The system does not experience tipping if

$$q(0, \epsilon) < q_{\text{crit}}(\epsilon) := q^b + \frac{1}{a_0} \sqrt{-\frac{\ddot{q}(0, \epsilon)}{2\kappa}} + o(\epsilon). \quad (6)$$

The first term added to  $q^b$  is of order  $\epsilon$  since  $\ddot{q}(0, \epsilon) = -\epsilon^2 R_2 + o(\epsilon^2)$ . The combination of the quantities  $a_0$  and  $\kappa$ , needed for (6),  $1/(a_0\sqrt{2\kappa})$ , may be found via the quantity

$$d := \frac{\partial}{\partial q} [(-\lambda(q))^2]|_{q=q^b} = \lim_{q \rightarrow q^b} \frac{[-\lambda(q)]^2}{q^b - q}, \quad (7)$$

where  $\lambda(q)$  is the leading eigenvalue of the linearization of underlying system (2) toward the stable equilibrium  $y^s(q)$  (or, equivalently, the decay rate toward  $y^s(q)$ ) in the original time-scale  $t_{\text{old}}$  and spatial scale  $\mathbf{y}$ . Then  $d = 4a_0^2\kappa$ , such that criterion (6) for avoiding tipping becomes

$$q(0, \epsilon) < q_{\text{crit}}(\epsilon) = q^b + \sqrt{-\frac{2\ddot{q}(0, \epsilon)}{d}} + o(\epsilon), \quad (8)$$

where both,  $d$  and  $\ddot{q}(0, \epsilon)$ , are computed in the original time scale. Thus, to establish the critical permissible distance  $\max_t q(\epsilon t, \epsilon) - q^b$  over the threshold before tipping, we need some estimate of the attraction rate toward the stable equilibria near the fold. This decay rate can, for example, be estimated through the autocorrelation in the output time series  $x(t)$  when the system is subject to fluctuations [20–22, 31].

Furthermore, for every  $R_0 > 0$  (or  $q(0, \epsilon) > q^b$ ) we can introduce an alternative parameter to  $\ddot{q}(0, \epsilon)$ : let the exceedance time  $t_e$  be the time that the parameter path  $q(\epsilon t, \epsilon)$  spends beyond the fold bifurcation value  $q^b$ . In the original time scale, the relationship between  $t_e$  and the other path parameters  $q(0, \epsilon)$  and  $\ddot{q}(0, \epsilon)$  is approximately

$$t_e = \sqrt{\frac{8(q^b - q(0, \epsilon))}{\ddot{q}(0, \epsilon)}} + O(1) = \sqrt{\frac{4R_0}{\epsilon R_2}} + O(1). \quad (9)$$

As the second expression makes clear, the exceedance time  $t_e$  is large (of order  $\epsilon^{-1/2}$ ), even when the amplitude of the exceedance  $\epsilon R_0 + O(\epsilon^2)$  is small. We can

then insert relation (9) into (8) to eliminate  $\ddot{q}(0, \epsilon)$  and establish the inverse-square law for maximal exceedance amplitude  $q(0, \epsilon) - q^b$  and time of exceedance  $t_e$  that avoids tipping. (recall that  $q(0) = \max_t q(t) =: q^{\max}$  and  $d$  is given by (7)):

$$d [q^{\max} - q^b] t_e^2 \leq 16, \text{ or, } a_0^2 \kappa [q^{\max} - q^b] t_e^2 \leq 4. \quad (10)$$

In applications the parameter path is typically not given in the form  $q(\epsilon t, \epsilon)$ , but rather as a simple function of time  $q(t)$ . The quantities  $d$ ,  $q^{\max} - q^b$  and  $t_e$  can be computed or estimated without explicitly introducing  $\epsilon$ . Then the above inequality is a valid criterion for the tipping threshold if  $q^{\max} - q^b$  is small in modulus, while  $t_e$  is large and the path is approximately parabolic in  $[-t_e, t_e]$ .

### III. INDIAN SUMMER MONSOON MODEL

We will focus on one of the recognised policy-relevant tipping elements in the Climate System, the Indian Summer Monsoon [1, 32]. The Indian economy and agriculture is heavily reliant on the Indian Summer Monsoon [33] as it provides the main source of water for India[34]. In the second half of the 20th century, summer rainfall has decreased leading to an increasing frequency of droughts [35], reducing rice harvests[36]. In particular, in 2002 India experienced a major drought with a seasonal rain deficit of 21.5% [33], seeing an increase in suicides amongst farmers and an estimated cost of 340 million dollars to the Indian government for drought relief programs [34]. Meehl *et al.* [37] connect these observations of decreased rainfall and increased droughts to an already present disruption of the monsoon.

We study a model for the Indian Summer Monsoon [13], which contains the key driving force of the monsoon, a moisture-advection feedback loop [12]. In the summer months the land is warmer than the ocean. This temperature difference generates winds coming off the Indian ocean onto the land. The winds carry moisture from the ocean which is deposited over the land in the form of precipitation. This process releases latent heat, meaning that the temperature over land increases. A larger temperature difference causes stronger winds carrying more moisture and hence the positive feedback loop is formed.

We use a model proposed by Zickfeld [11] and make further simplifications, though retaining the key mechanism of the monsoon, the positive feedback loop described above. Two components, the specific humidity  $Q_a$  and the atmospheric temperature  $T_a$ , are described by the following ODEs:

$$\dot{Q}_a = \frac{E - P + A_v}{\beta I_q}, \quad (11)$$

$$\dot{T}_a = \frac{\mathcal{L}(P - E) - F_{\uparrow}^{LW,TA} + F_{\downarrow}^{SL,TA}(1 - A_{\text{sys}}) + A_T}{\beta I_T} \quad (12)$$

where the terms on the right-hand side are grouped as follows:

- Evaporation  $E$  (mm/s): Proportional to the temperature difference between the land  $T_a$  and the Indian Ocean  $T_{oc}$  and to the difference between saturated humidity  $Q_{\text{sat}}$  and specific humidity  $Q_a$

$$E := E(Q_a, T_a) = C_E(T_a - T_{oc})(Q_{\text{sat}} - Q_a).$$

- Precipitation  $P$  (mm/s): Proportional to the specific humidity

$$P := P(Q_a) = C_P Q_a.$$

- Moisture advection  $A_v$  (mm/s): Winds driven by the temperature difference between the land and ocean bring moisture from the ocean over land proportional to the humidity over the ocean  $Q_{oc}$ . Winds are reversed above a given height taking moisture away proportional to the humidity over land  $Q_a$

$$A_v := A_v(Q_a, T_a) = (T_a - T_{oc})(C_{mo}Q_{oc} - C_{ml}Q_a).$$

- Outgoing long-wave radiation  $F_{\uparrow}^{LW,TA}$  (kg/s<sup>3</sup>): Proportional to the temperature of the land

$$F_{\uparrow}^{LW,TA} := F_{\uparrow}^{LW,TA}(T_a) = C_{L1}T_a + C_{L2}.$$

- Incoming short-wave radiation  $F_{\downarrow}^{SL,TA}$  (kg/s<sup>3</sup>): Fraction of incoming solar radiation not reflected, proportional to  $1 - A_{\text{sys}}$ , where  $A_{\text{sys}}$  is the system planetary albedo.

- Heat advection  $A_T$  (kg/s<sup>3</sup>): Winds driven by the temperature difference between the land and ocean bring cool air at a prescribed low altitude proportional to the potential temperature  $\theta_{oc}$  above the ocean ( $\theta_{oc}$  is fixed). Reversed winds at a prescribed high altitude  $z_h$  take warm air away proportional to the potential temperature above the land  $\theta_a(Q_a, T_a)$ . The potential temperature at the prescribed height  $z_h$  is given by  $\theta_a = T_a - (\Gamma(T_a, Q_a) - \Gamma_a)z_h$  where  $\Gamma = \Gamma_0 + \Gamma_1(T_a - T_0)(1 - \Gamma_2 Q_a^2)$  (with a reference temperature  $T_0$ ) is the atmospheric lapse rate and  $\Gamma_a$  is the adiabatic lapse rate

$$A_T := A_T(Q_a, T_a) = C_H(T_a - T_{oc})(\theta_{oc} - \theta_a(Q_a, T_a)).$$

The remaining terms are all constants, in particular, latent heat is given by  $\mathcal{L}$ , and  $\beta$  provides a conversion from seconds to decades (the unit of time  $t$  is decades). Appendix B, Table I lists all parameters and their values and units.

Zickfeld *et al.* [13] identified two quantities that are influenced by human activities or subject to natural variation and affect the stability of the monsoon. Either an increase of the planetary albedo  $A_{\text{sys}}$  or a decrease in the  $CO_2$  concentration from present day values can potentially lead to a “shutdown” of the Indian monsoon. We

will focus our analysis on the possibility of an increase in the planetary albedo.

The planetary albedo represents the ratio of reflected to incoming solar radiation and can be influenced by atmospheric aerosols and land-cover conversion [13]. In particular, the atmospheric brown cloud haze hanging over the Indian subcontinent has been considered responsible for the disruption of the monsoon with some future projections suggesting the drought frequency could double within a decade [35]. This cloud haze is predominately made up of black carbon aerosols emanating from fossil fuel combustion and biomass burning, which both absorb and reflect (thus, increasing planetary albedo) incoming radiation [37]. Knopf *et al.* [38] have previously performed a multi-parameter uncertainty analysis for the original Zickfeld model, which models the planetary albedo as a function of the surface albedo. They concluded that if the model is reliable the bifurcation point for the surface albedo is sufficiently far from present day values such that this point cannot be reached in the near future. However, brown haze is typically poorly captured by the functional dependency assumed in the models [1]. Thus, the pollution-driven changes such as brown haze may place the monsoon system closer to its bifurcation point than concluded by Knopf *et al.* [38]. On a positive note this pollution is a regional problem, so does not require any world-wide agreement [34] and therefore reversion of tipping by rapid action may be politically more feasible [32].

Zickfeld *et al.* [13] states that the present day value of the planetary albedo is  $A_{\text{sys}}^{\infty} = 0.47$ , which is consistent with satellite data, from 2000-2012, which suggests an averaged summer value of around 0.45 for India [39]. System (11)–(12) has a fold (saddle-node) bifurcation at  $A_{\text{sys}}^b \approx 0.53$ , see Figure 1b. Slowly increasing the planetary albedo linearly beyond the fold will cause tipping in the monsoon model, a sudden drop in the specific humidity would be observed. Equation (12) highlights how increasing the planetary albedo affects the positive feedback loop outlined above. As the albedo is increased, the change in temperature over land decreases, meaning a smaller temperature difference between the land and ocean and hence weaker winds are formed. Our aim is to study how long the planetary albedo can be kept above the fold bifurcation parameter value  $A_{\text{sys}}^b$  without causing a tipping of the Indian Summer Monsoon. Therefore we choose to force the planetary albedo as detailed in Section II, namely

$$A_{\text{sys}}(t) = A_{\text{sys}}^{\infty} + \frac{R + A_{\text{sys}}^b - A_{\text{sys}}^{\infty}}{\cosh(\epsilon(t_{\text{end}} - 2t))^2} \quad (13)$$

for a time interval  $[0, t_{\text{end}}]$ . Equation (13) describes increasing the planetary albedo towards (and possibly beyond) the fold bifurcation before it returns to its present day value. Three time profiles of the planetary albedo forcing (13) are given in Figure 1a for illustration. All three fix the speed of path traversal  $\epsilon = 0.5$ , and vary  $R$ , the difference between maximal albedo and its bifurca-

tion value  $A_{\text{sys}}^b$ . The exceedance  $R$  of the maximal albedo beyond the fold bifurcation value  $A_{\text{sys}}^b$  (indicated by the horizontal dashed line) and the time  $t_e$  the albedo  $A_{\text{sys}}(t)$  spends above  $A_{\text{sys}}^b$  are controlled by  $\epsilon$  and  $R$  via

$$t_e = \frac{1}{2\epsilon} \sqrt{\frac{R}{A_{\text{sys}}^b - A_{\text{sys}}^\infty}} + O(R^{3/2}/\epsilon).$$

The trajectories for each forcing are superimposed on top of the bifurcation diagram for fixed  $A_{\text{sys}}$  in Figure 1b.

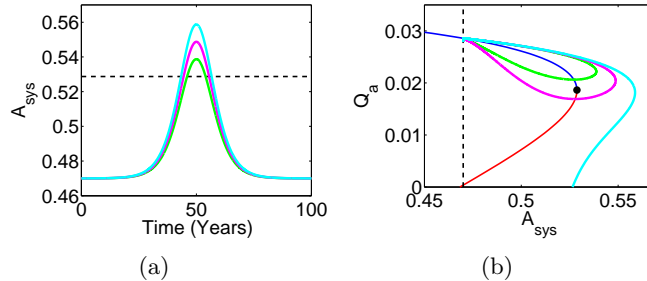


FIG. 1: (a) Time profiles of planetary albedo forcing (13) for  $R = 0.01$  (green),  $R = 0.02$  (pink) and  $R = 0.03$  (bright blue) but fixed  $\epsilon = 0.5$ , proportional to the time period. Horizontal dotted line indicates location  $A_{\text{sys}}^b$  of the fold bifurcation. (b) Bifurcation diagram of (11)–(12) in the  $(A_{\text{sys}}, Q_a)$  - plane. Upper branch stable (blue) and lower branch is unstable (red). Superimposed on top are trajectories starting at  $A_{\text{sys}}^\infty = 0.47$  (vertical dotted line) close to the stable equilibrium branch and subjected to the planetary albedo forcing given in (a).

The green trajectory corresponds to a forcing scenario where the system parameter is increased just beyond the fold before decreasing again. In this scenario the system has little time to escape before the stable branch re-emerges. Increasing  $A_{\text{sys}}$  further beyond its bifurcation value  $A_{\text{sys}}^b$ , the trajectory (shown in pink) begins to escape such that when the branches of equilibria reappear the trajectory is initially on the other side of the unstable branch. However, the system recovers fast enough for the trajectory to cross the unstable branch and be attracted back to the stable branch. The final case (bright blue) the planetary albedo is forced sufficiently far beyond the fold bifurcation  $A_{\text{sys}}^b$  such that the system is unable to recover quickly enough to prevent tipping.

We can calculate numerically the critical curve separating a “safe” area (monsoon retained) from the “unsafe” area, where escape toward shutdown occurs, in the two-parameter plane. We choose as path parameters the peak exceedance beyond the fold  $R$ , and exceedance time  $t_e$ .

The critical parameters, for which the exact (numerically computed) connecting orbit to the saddle occurs, are shown as a blue solid curve in Figure 2. As discussed in Section II, the critical amount by which the planetary albedo exceeds the fold value  $A_{\text{sys}}^b$  is approximately inversely proportional to the square of the time

the planetary albedo stays above  $A_{\text{sys}}^b$ . For example, if the planetary albedo is forced only just above the bifurcation ( $R = 0.005$ ) then the system can spend a long time ( $\sim 30$  years) above the bifurcation value without shutting down the monsoon. However, for a higher maximum of  $A_{\text{sys}}$  ( $R = 0.02$  above the bifurcation value) the system can maintain the monsoon only if the exceedance time  $t_e$  is shorter ( $\sim 15$  years).

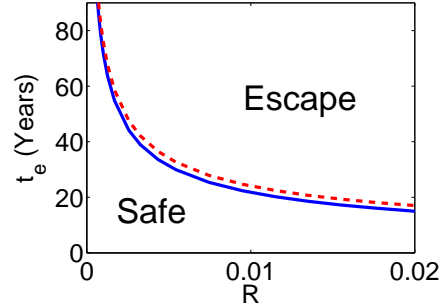


FIG. 2: Tipping region in the two parameter plane  $R = \max_t A_{\text{sys}}(t) - A_{\text{sys}}^b$  (Peak distance over fold (saddle-node)) and  $t_e$  (Time above fold). Safe region and escape region separated by the numerically calculated critical curve (blue solid). The red dashed curve provides an approximation of the critical curve obtained from equation (10), where  $d = 318.36$  per decades<sup>2</sup>.

The parameter values satisfying the theoretical inequality (10) (valid for the limit  $\epsilon \rightarrow 0$ ) are below the red dashed curve in Figure 2. The curve gives a good approximation to the numerically calculated critical curve. The approximation is best for small critical  $R$  (peak distance over fold) because then the system spends most time in the region of the phase space where the second-order expansion of the right-hand side in the fold and of the path in its maximum are valid (both of these were assumed in the derivation of inequality (10)).

#### IV. PROBABILITY OF TIPPING UNDER THE INFLUENCE OF NOISE

In this section we study the probability of tipping when the system is, in addition to its parameter drift, subject to random disturbances, which we model by adding white noise to (2). We again consider a parameter path satisfying conditions P1–P3, touching a fold satisfying conditions S1–S5. We focus on the case where the disturbances are sufficiently small such that escape is unlikely at times when the parameter path  $q(\epsilon t, \epsilon)$  is away from its maximum (for  $|t| \gg 1/\epsilon$ ). Close to the fold the decay rate in the center direction  $\mathbf{v}_0$  is much smaller than the decay rates in the stable directions  $\mathbf{y}_s$  (defined by  $\mathbf{w}_0^T \mathbf{y}_s = 0$ ), such that disturbances entering through coupling between stable and center directions are small. If

the  $n$ -dimensional noise has covariance matrix  $\Delta$ , its projection along direction  $\mathbf{w}$  onto the scalar output, after the rescaling (3) to the zoomed-in output  $x = \epsilon^{1/2} \mathbf{w}^T (\mathbf{y} - \mathbf{y}^b)$  and sped up time, has the variance  $\epsilon^{-3/2} \mathbf{w}_0^T \Delta \mathbf{w}_0$ . Hence, if the variance of the projected additive noise is larger than  $O(\epsilon^{3/2})$  the probability of escape will approach 1 for  $\epsilon \rightarrow 0$ .

Consequently, we assume that the variance of the noise is of order  $\epsilon^{3/2}$  in the original coordinates and focus on the vicinity of the fold, where the rescaled noise variance

$$2D := 2\epsilon^{-3/2} \mathbf{w}_0^T \Delta \mathbf{w}_0 \quad (14)$$

is now of order 1. Thus, in the limit for  $\epsilon \rightarrow 0$ , the projected equation (4) becomes the scalar stochastic differential equation (SDE)

$$dx = a_0[R_0 - R_2 t^2 + \kappa x^2]dt + \sqrt{2D}dW_t \quad (15)$$

(recall that  $a_0 > 0$  and  $\kappa > 0$  without loss of generality). By further rescaling  $x$  and time and introducing correspondingly rescaled versions of the parameters  $R_0$  and  $R_2$ ,

$$\begin{aligned} x_{\text{new}} &= \frac{(a_0 \kappa)^{1/3}}{D^{1/3}} x_{\text{old}}, \quad t_{\text{new}} = D^{1/3} (a_0 \kappa)^{2/3} t_{\text{old}}, \\ p_0 &= \frac{a_0^{2/3}}{D^{2/3} \kappa^{1/3}} R_0, \quad p_2 = \frac{R_2}{D^{4/3} \kappa^{5/3} a_0^{2/3}}, \end{aligned} \quad (16)$$

we may simplify (15) to a SDE

$$dx = [p_0 - p_2 t^2 + x^2]dt + \sqrt{2}dW_t \quad (17)$$

with unit noise amplitude and nonlinear coefficient, and the two parameters  $p_0 \in \mathbb{R}$  and  $p_2 > 0$ . The lines

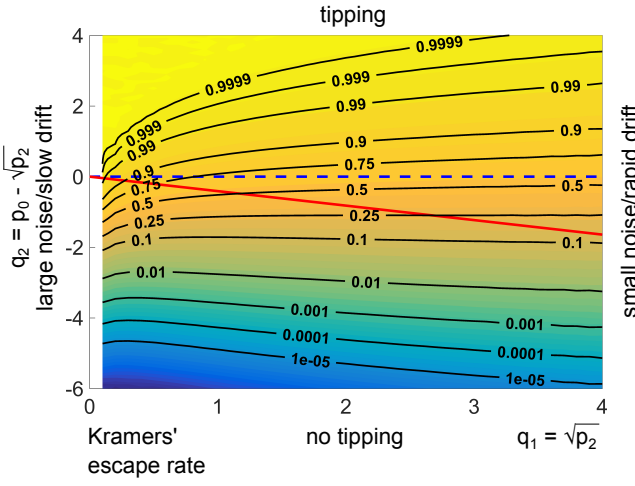


FIG. 3: Probability of escape  $P_{\text{esc}}$  to  $+\infty$  in (17) for intermediate parameter values of  $q_1 = \sqrt{p_2}$  and  $q_2 = p_0 - \sqrt{p_2}$ . Parameters for FPE (18): domain  $[-8, 8]$ , time interval  $[-T_0, T_0]$ , initial density  $N(x_0, 1)$  where  $T_0 = \sqrt{(x_0^2 + p_0)/p_2}$  and  $x_0 = -4$ .

$x = \sqrt{p_2}t$  for  $t \ll -1$  and  $x = -\sqrt{p_2}t$  for  $t \gg 1$  are stable

slow manifolds of the deterministic part of (17). Thus, the density of  $x$  at some fixed large time  $t = -T_0$  is nearly independent from the initial density for  $t \ll -T_0$  (conditional on no escape occurring before  $t = -T_0$ ). Thus, we can compute numerically the probability of escape by solving the Fokker-Planck equation (FPE) for the density  $u(x, t)$  of  $x$

$$\partial_t u(x, t) = \partial_x^2 u(x, t) - \partial_x[(p_0 - p_2 t^2 + x^2)u(x, t)] \quad (18)$$

with Dirichlet boundary conditions  $u(t, x_{\text{bd}}) = u(t, -x_{\text{bd}}) = 0$  from  $t = -T_0$  to  $t = +T_0$ , starting from an arbitrary density concentrated in the region  $\{x \leq 0\}$  and a sufficiently large  $T_0$ . The resulting escape probability  $P_{\text{esc}}(p_0, p_2)$  is then (approximately for large  $T_0$  and large  $x_{\text{bd}}$ ) given by

$$P_{\text{esc}}(p_0, p_2) = 1 - \int_{-x_{\text{bd}}}^{x_{\text{bd}}} u(x, T_0)dx. \quad (19)$$

The result (using `chebfun` [40]) in the coordinates  $q_1 = \sqrt{p_2} \in [0.1, 4]$ , and  $q_2 = p_0 - \sqrt{p_2} \in [-6, 4]$  is shown in Figure 3.

When one varies the noise variance  $D$  in the original system (15), keeping the original path parameters  $R_0$  and  $R_2$  fixed, one moves along a straight line through the origin in Figure 3. An example is shown by a red line in Figure 3. The small-noise limit is at the large- $p_2$  (or  $q_1$ ) end, and the large noise (or slow drift) limit is at the origin.

In the coordinates  $(q_1, q_2) = (\sqrt{p_2}, p_0 - \sqrt{p_2})$  the slope of all  $P_{\text{esc}}$  level curves of equal probability will approach 0 for large  $q_1$  (or  $\sqrt{p_2}$ ) such that the level curve for  $P_{\text{esc}} = 0.5$  asymptotes to the horizontal  $q_2 = p_0 - \sqrt{p_2} = 0$  as at these parameter values the deterministic system has its tipping threshold (see (5) in Section II), and the limit of large  $p_2$  (or  $q_1$ ) corresponds to the rapid drift (or small noise) limit. The  $q_2$  coordinate of the  $P_{\text{esc}}$  level curves for  $P_{\text{esc}} < 0.5$  decreases slightly faster than logarithmic in  $q_1$ , while for  $P_{\text{esc}} > 0.5$  levels the  $q_2$  coordinate increases (slightly faster than logarithmically) for increasing  $q_1$ .

While the numerical result is sufficient for some practical estimates, Appendix A gives approximation formulas for some regions of the  $(q_1, q_2)$  plane, which may provide additional insight into the nature of various terms and better accuracy in the region of small  $q_1 = \sqrt{p_2}$ .

In the parameter region below the red line  $q_2 = -0.41q_1$  in Figure 3, a reasonable approximation of the escape rate at time  $t$  is provided by the leading eigenvalue  $-\gamma_1(\bar{x})$  of the Fokker-Planck operator  $[F_{\bar{x}}u](z) := \partial_z^2 u(z) - \partial_z[(z^2 + 2\bar{x}z)u(z)]$  with Dirichlet boundary conditions for large  $z$  at both ends. The value of  $\bar{x}$  at time  $t$  for parameters  $p_0$  and  $p_2$ ,  $\bar{x}(t; p_0, p_2)$ , is the unique solution of  $\dot{x} = p_0 - p_2 t^2 + x^2$  with  $\bar{x}(t; p_0, p_2) + \sqrt{p_2}|t| \rightarrow 0$  for  $|t| \rightarrow \infty$  (see Appendix A for details). This permits us to estimate escape probabilities after a one-off fit of the leading eigenvalue  $-\gamma_1(\bar{x})$ :

$$P_{\text{esc}}^{1d} \approx 1 - \exp \left( \int_{-\infty}^{\infty} \gamma_1(\bar{x}(t; p_0, p_2)) dt \right). \quad (20)$$

For (20), a crude fit for  $\gamma_1(\bar{x})$  is  $\gamma_{1,2}(\bar{x}) = \exp(-c_0 - c_2 \bar{x}^2)$  with  $c_0 = 1.01$  and  $c_2 = 1.41$ ; see Appendix A for a graph in Fig. 7b and a better fit. A necessary condition for the accuracy of the approximation is that  $\bar{x}(t; p_0, p_2) < 0$  for all  $t$ , which is the case below the red line in Figure 3.

## V. PROBABILITY OF TIPPING FOR THE MONSOON MODEL

We now estimate the probability of tipping for the Monsoon model by projecting the system (11,12) onto a one-dimensional output ( $\mathbf{w}^T = \mathbf{w}_0^T = (-3.50, -0.99)$ ) and expanding it near the fold to quadratic order (in  $x$ ), and using (20). If time is measured in decades, the quadratic expansion of the monsoon model near its fold has the form  $\dot{x} = p_f(A_{\text{sys}}(t) - A_{\text{sys}}^b) + x_f x^2$  where  $x$  is a dimensionless projection of the state. We add white noise of variance  $2\Delta = \text{diag}(0.02, 6)$  to the monsoon model (11)–(12), such that

$$dx = [p_f(A_{\text{sys}}(t) - A_{\text{sys}}^b) + x_f x^2]dt + \sqrt{2D}dW_t \quad (21)$$

with  $p_f = 115.30$ ,  $x_f = 0.69$ ,  $D = 3.04$ . The paths  $A_{\text{sys}}(t)$  are chosen identical to equation (13)

$$A_{\text{sys}}(t) = A_{\text{sys}}^\infty + \frac{R^{(0.5)} + A_{\text{sys}}^{\text{th}} - A_{\text{sys}}^\infty}{\cosh(\epsilon(t_{\text{end}} - 2t))^2}, \quad (22)$$

where  $A_{\text{sys}}^\infty = 0.47$  is the present-day value of the albedo and  $[0, t_{\text{end}}]$  is the time interval. Since in the probabilistic scenario, tipping is possible also for paths  $A_{\text{sys}}(t)$  that do not exceed  $A_{\text{sys}}^b$ , it is useful to also consider other (especially lower) thresholds than  $A_{\text{sys}}^b$  for measuring exceedance amplitudes and times. We choose  $A_{\text{sys}}^{\text{th}} = 0.5$ , and, hence, consider the parameter plane  $(R^{(0.5)}, t_e^{(0.5)})$ , where  $R^{(0.5)} = R + A_{\text{sys}}^b - 0.5$  is the distance of the maximal albedo along the path from a chosen albedo threshold  $A_{\text{sys}}^{\text{th}} = 0.5$ , and  $t_e^{(0.5)}$  is the corresponding exceedance time above this threshold.

Figure 4 shows the single mode approximation (20) for the solution  $\bar{x}$  of (21)–(22) for the probability of tipping  $P_{\text{esc}}^{\text{1d}}$ , (a fit for  $\gamma_1(\bar{x})$  is given in Appendix A), on a grid of points in this  $(R^{(0.5)}, t_e^{(0.5)})$ -plane. Since the mode approximation (20) is valid only in the region  $q_2 < -0.41q_1$  (below the red line in Figure 3), Figure 4 leaves a part of the  $(R^{(0.5)}, t_e^{(0.5)})$ -plane white. The vertical white dashed line positioned indicates the location of the deterministic fold bifurcation and the black dashed curve provides the boundary for deterministic ( $D = 0$ ) tipping.

The results in Figure 4 show that the level curves for equal probability align with the inverse-square law for deterministic tipping only partially, namely in those parameter regions that correspond to  $q_1$  and  $q_2$  with nearly horizontal level curves in Figure 3. For  $R^{(0.5)} < 0.02$  (meaning that the fold (saddle-node) is not reached) and small  $t_e^{(0.5)}$  (fast shifts) the probability of tipping is small.

The probability of tipping increases if the path exceeds the fold ( $R^{(0.5)} > 0.03$ ) or the exceedance time  $t_e^{(0.5)}$  over the threshold increases. Note that the  $(R^{(0.5)}, t_e^{(0.5)})$  coordinates are singular at their origin such that all equal-probability level curves pass through the origin. In Ap-

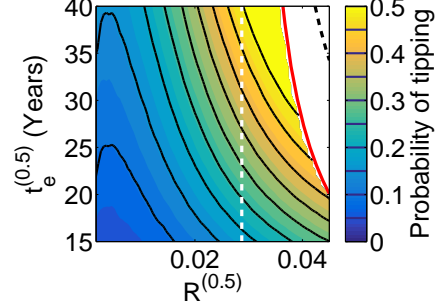


FIG. 4: Contour of the probability of tipping (20), using the leading eigenvalue  $\gamma_1$  in the  $(R^{(0.5)}, t_e^{(0.5)})$ -plane. Contour lines are spaced at 0.05 intervals. White dashed line indicates the fold bifurcation, black dashed curve shows the critical parameter values for deterministic tipping and the red solid curve indicates the boundary for validity of the mode approximation.

Parameters:  $\mathbf{w} = (-3.50, -0.99)^T$  such that  $p_f = 115.30$  and  $x_f = 0.69$  in (21),  $D = 3.04$ .

pendix A, we compare the mode approximation (20), which uses only the leading eigenvalue  $\gamma_1$  of the Fokker-Planck equation for the one-dimensional projection (21), to the true probability of tipping for the full 2d system (11)–(12).

Figure 5b shows the probability of tipping for a range of times  $t_e^{(0.5)}$  for which  $A_{\text{sys}}(t)$  is above the threshold 0.5 for two fixed maxima  $\max_t A_{\text{sys}}(t)$ . Figure 5a shows example forcing paths  $A_{\text{sys}}(t)$  for two different exceedance times for each fixed maximum.

## VI. SUMMARY

In this paper, we have investigated the scenario of forcing a system over a tipping threshold (a fold of equilibria) for a short time. We provide simple criteria determining whether the forced deterministic system escapes from the family of equilibria or not. The two primary parameters of the forcing path  $q(t)$  are the maximum exceedance amplitude  $\max_t q(t)$  of the fold bifurcation parameter value  $q^b$  and the time  $t_e$  for which the parameter path has exceeded the fold bifurcation value. The critical curve, which separates a region of tipping and the safe region in this two-parameter plane follows an inverse-square law:  $t_e^2(\max_t q(t) - q^b) = 16/d$ . The constant  $d$  can be determined from equilibria at parameters  $q$  near the critical value  $q^b$  as the ratio of the square of the decay rate to  $q - q^b$ .

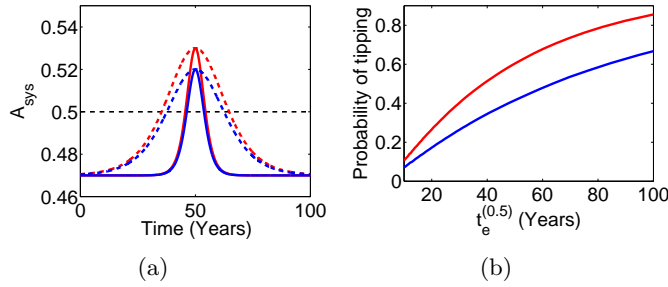


FIG. 5: Cross sections in Figure 4 for two different values of  $R^{(0.5)}$ :  $R^{(0.5)} = 0.02$  (blue) and  $R^{(0.5)} = 0.03$  (red). (a) Time profiles of planetary albedo forcing paths of a short (solid) and longer (dashed) exceedance time  $t_e^{(0.5)}$  for each fixed  $R^{(0.5)}$  value. Horizontal black dotted line represents the chosen threshold value  $A_{\text{sys}} = 0.5$  used for the definition of  $R^{(0.5)}$  and  $t_e^{(0.5)}$ . (b) Probability of tipping over a range of exceedance times (times for which  $A_{\text{sys}}$  is larger than 0.5).

We used a simplified version of the Indian Summer Monsoon model developed by Zickfeld [11] to demonstrate which time profiles for changing planetary albedo in the model result in (or avoid) tipping, matching the general theoretical predictions (which are only accurate if one is sufficiently close to a fold) precisely: the trade-off between exceedance amplitude and time beyond the critical value of the albedo follows the inverse-square law.

We also quantify the effect of random disturbances, modelled by white additive noise, determining a probability of tipping. For each chosen threshold  $q_0$  near the fold we obtain level curves of equal probability in the parameter plane  $(\max_t q(t) - q_0, t_e^0)$  of exceedance amplitude and exceedance time for  $q_0$ . These level curves follow the inverse-square law in part, deviating from it (expectedly) in the large-noise (slow-drift) limit and at the origin of the  $(\max_t q(t) - q_0, t_e^0)$ .

## ACKNOWLEDGMENTS

P.R.'s research was supported by funding from the EPSRC Grant No. EP/M008495/1, P.R. has also received funding from the NERC grant No. NE/P007880/1. J.S. gratefully acknowledges the financial support of the EPSRC via Grants No. EP/N023544/1 and No. EP/N014391/1. J.S. has also received funding from the European Union's Horizon 2020 research and innovation programme under Grant Agreement No. 643073. We would like to thank Tim Lenton for advice on the current consensus on the prospects of tipping in the Indian Summer Monsoon. The research materials supporting this publication can be accessed at <https://doi.org/10.6084/m9.figshare.5492914>

## Appendix A: Approximations of tipping probability $P_{\text{esc}}$

This appendix discusses different approximation methods used for calculating the tipping probability  $P_{\text{esc}}$  for various regions of the  $(q_1, q_2)$  plane.

The double exponential of  $1 - P_{\text{esc}}$  satisfies a cubic fit accurately over the region shown in Figure 3:

$$1 - P_{\text{esc}} \approx \exp \left[ -\exp \sum_{k=0, j \leq k}^3 c_{kj} q_1^j q_2^{k-j} \right], \quad (\text{A1})$$

where the coefficients  $c_{kj}$  are given in Table II. The absolute error over the region of Figure 3 is 0.024 and the cut-off relative error  $(|P_{\text{esc}} - P_{\text{esc}}^{\text{approx}}| / \max(0.1, P_{\text{esc}}))$  is less than 10%.

*a. Slow drift approximation* For small parameters  $p_2$  (or  $q_1$ ) the integration of the FPE (18) would require long time intervals (only for times of order  $1/\sqrt{p_2}$  are well separated stable and unstable slow manifolds present in the deterministic part  $\dot{x} = p_0 - p_2 t^2 + x^2$ ). However, in this regime the time-dependence of the SDE (17) is weak: the time derivative of the right-hand side  $p_0 - p_2 t^2 + x^2$  is of order  $\sqrt{p_2}$  for  $|t| \sqrt{p_2}$  or order 1 or less. Hence, we may approximate the rate of escape at each time  $t$  using the escape rate for the static potential well corresponding to the right-hand side  $p_0 - p_2 t^2 + x^2$ . This escape rate is given by the dominant eigenvalue  $\lambda_0$  of the linear operator on the right-hand side of the Fokker-Planck equation (18). Solving the parameter-dependent eigenvalue problem

$$-\lambda(p)u(x, p) = \partial_x^2 u(x, p) - \partial_x[(p + x^2)u(x, p)] \quad (\text{A2})$$

for its first eigenvalue  $\lambda_0$  (specifically, with Dirichlet boundary conditions on the interval  $[-8, 8]$  using `chebfun`[40]), provides the escape rate. The eigenvalue

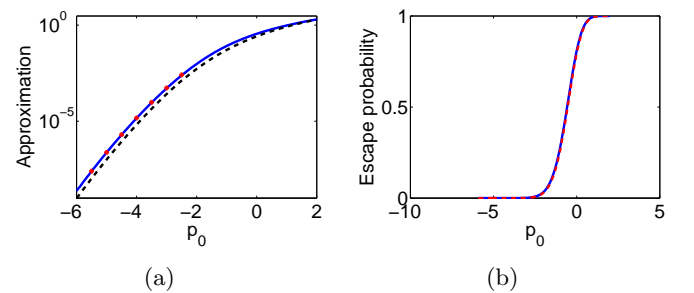


FIG. 6: Slow drift approximation: (a) shows the leading eigenvalue  $\lambda_0(p)$  (blue solid) as numerically computed using (A2), the approximation given by Kramers' escape rate (red markers) and  $\mu_0$  defined in (A3). (b) compares the slow drift approximation (A3) (blue solid) to the numerical value (from Figure 3) (red dashed) at  $p_2 = 0.1$ . The difference always below 0.02.

$\lambda_0(p)$  is real and positive (due to the minus sign on

the left-hand side in (A2)), and exponentially small for  $p \ll -1$ , where the approximation with Kramers' escape rate ( $\lambda_0 \approx \sqrt{-p}/\pi \exp(4p\sqrt{-p}/3)$  for the drift term in (A2) and  $D = 1$ ) is valid. Figure 6a shows  $\lambda_0$  and the Kramers' escape rate approximation. The probability of *not* escaping is then the product of all probabilities of not escaping near all times  $t$ , such that overall:

$$\begin{aligned} P_{\text{esc}} &\approx 1 - \exp \left( -2 \int_0^\infty \lambda_0(p_0 - p_2 t^2) dt \right) \\ &\approx 1 - \exp \left( -2p_2^{-1/2} \mu_0(p_0) \right) \end{aligned} \quad (\text{A3})$$

where  $\mu_0(p) = \int_0^\infty \lambda_0(p_0 - s^2) ds$  is also shown in Figure 6a. Since the eigenvalue  $\lambda_0(p)$  (and its integral  $\mu_0(p)$ ) are exponentials, approximation (A3) explains the double exponential nature of the probability  $P_{\text{esc}}$ . The logarithms of  $\lambda_0$  and  $\mu_0$  fit accurately to cubic polynomials over the range shown in Figure 6 ( $\mu_0(p) \approx \exp(1.35(p-1))$  fits up to 0.02 in absolute value for  $p < 0.3$ ; see Table II). Figure 6b compares the slow-drift approximation (A3) to the numerical result from Figure 3. The absolute error is always below 0.02 and the cut-off relative error ( $|P_{\text{esc}} - P_{\text{esc}}^{\text{slow}}| / \max(0.1, P_{\text{esc}})$ ) is less than 10%. The slow drift approximation becomes more accurate for values of  $p_2$  smaller than 0.1.

*b. Single mode approximation in moving coordinates*  
An approach explored by Ritchie and Sieber [41] extends the slow drift approximation to a region of the parameter plane where  $p_2$  is not small. We consider the unique solution  $\bar{x}(t; p_0)$  of the deterministic ODE (dropping  $\sqrt{2}dW_t$  from (17))

$$dx(t) = [p_0 - p_2 t^2 + x(t)^2] dt \quad (\text{A4})$$

satisfying  $\bar{x}(t; p_0) + \sqrt{p_2}|t| \rightarrow 0$  for  $t \rightarrow \infty$  (see Figure 7a). Then we make a time-dependent coordinate shift  $z(t) = x(t) - \bar{x}(t; p_0, p_2)$  and consider escape of a realization of  $z$  from the vicinity of the origin when adding stochastic disturbances to this shifted system:

$$dz = [z^2 + 2\bar{x}(t; p_0, p_2)z] dt + \sqrt{2}dW_t. \quad (\text{A5})$$

Now we apply the slow-drift approximation in the coordinate system for  $z$  (after the time-dependent shift). The eigenvalue problem for the operator on the right-hand side of the Fokker-Planck equation for (A5) is now (with Dirichlet boundary conditions)

$$-\gamma(p)u(z; p) = \partial_z^2 u(z; p) - \partial_z[(z^2 + 2pz)u(z; p)], \quad (\text{A6})$$

where the parameter  $p$  is equal to  $\bar{x}(t; p_0, p_2)$ . Ritchie and Sieber [41] give a way to approximate the escape rate  $\gamma_1(p)$ . Its numerically computed value is shown in Figure 7b (computation performed with `chebfun`[40] on the interval  $[-8, 8]$ ). As one can see, the escape rate  $\gamma_1(p)$  has a maximum at  $p = 0$ . This points to a limitation of the validity for the mode approximation. When the deterministic trajectory  $\bar{x}(t)$  enters the region

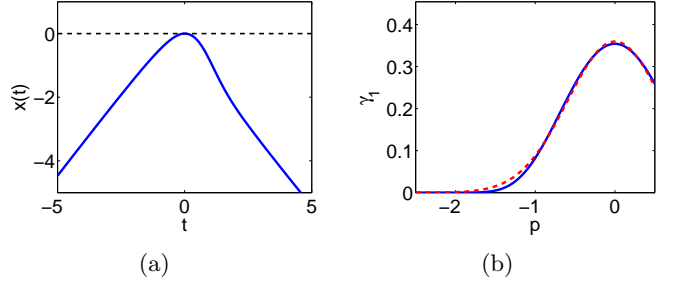


FIG. 7: (a) Trajectory of deterministic system (A4) with  $p_0 = 0.59$  and  $p_2 = 1$ . (b) Slow drift approximation (blue solid) and numerical value (red) of escape rate  $\gamma_1(p)$  for escape problem (A6).

$x > 0$ , it becomes locally repelling, such that the potential  $-z^3/3 - pz^2$  corresponding to (A5) has a hill top at 0, but a well at  $-2\bar{x}$ . The region of validity for the mode approximation is thus limited to the region where  $p = \bar{x} \leq 0$ . This implies that the deterministic reference trajectory  $\bar{x}(t; p_0, p_2)$  has to lie in  $\{x \leq 0\}$  for all  $t$ . This is the case when  $p_0 \leq 0.59\sqrt{p_2}$  (corresponding to the area below the red line in Figure 3).

Figure 7b also shows a fitted curve of the form  $\gamma_{1,2}(\bar{x}) = \exp(-c_0 - c_2\bar{x}^2)$  with  $c_0 = 1.01$  and  $c_2 = 1.41$ . A 4th-order fit  $\gamma_{1,4}(\bar{x}) = \exp\left(-\sum_{j=0}^4 c_j \bar{x}^{4-j}\right)$  with  $c = (0.33, 0.04, 1.17, -0.01, 1.04)$  has an absolute error less than  $10^{-3}$  and a cut-off relative error ( $|\gamma_1(p) - \gamma_{1,4}(p)| / \max(0.1, \gamma_1)$ ) less than  $10^{-2}$ .

Again, the probability of *not* escaping is the product of all probabilities of not escaping near all times  $t$ , such that overall

$$P_{\text{esc}} \approx 1 - \exp \left( - \int_{-\infty}^\infty \gamma_1(\bar{x}(t; p_0, p_2)) dt \right), \quad (\text{A7})$$

which equals the approximation (20) in Section IV. In contrast to the slow drift approximation (A3) the integrand  $\gamma_1$  depends on the deterministic trajectory  $\bar{x}(t; p_0, p_2)$ . This trajectory is typically non-symmetric about  $t = 0$  (see Figure 7a; in contrast to the simple parabolic path  $p_0 - p_2 t^2$ ) such that the escape rate has to be integrated over all times. As there is no good approximation formula for the trajectory  $\bar{x}(t; p_0, p_2)$  (a quadratic approximation at its maximum is typically poor), the integral has to be evaluated numerically. This evaluation can be performed in parallel to the computation of the trajectory  $\bar{x}(t; p_0, p_2)$  itself. For the normal form this would be an extension of the form (assuming that the integration interval is  $[-T_0, T_0]$ )

$$\dot{x} = p_0 - p_2 t^2 + x^2, \quad x(-T_0) = -T_0 \quad (\text{A8})$$

$$\dot{\gamma}_{\text{acc}} = \gamma_{1,4}(x), \quad \gamma_{\text{acc}}(-T_0) = 0. \quad (\text{A9})$$

Then  $P_{\text{esc}} \approx 1 - \exp(-\gamma_{\text{acc}}(T_0))$ . More generally, the parameter path does not have to be parabolic:  $p_0 - p_2 t^2$  may be replaced with an arbitrary function  $p(t)$  satisfying

$p(t) \ll -1$  for  $|t| \gg 1$  (after rescaling). Moreover,  $x$  in (A9) can be the rescaled scalar output of the simulated large system (after applying scalings (3) and (16):  $x(t) = \epsilon^{-1/2} D^{1/3} (a_0 \kappa)^{-1/3} w^T (y(t) - y^b)$ ). The initial condition for  $\gamma_{\text{acc}}$  should be set to 0, as (A9) evaluates the integral in (A7).

*c. Accuracy of projection and approximation* The projection to a one-dimensional system gives only accurate predictions for sufficiently small  $\epsilon$ , that is, for sufficiently small noise and slow parameter drift. We compare the predictions from the mode approximation of the projection onto the atmospheric temperature  $T_a$  to the results of the two-dimensional monsoon model (11)–(12). To evaluate the tipping probability for the two-dimensional monsoon model we solve the Fokker-Planck equation

$$\begin{aligned} \partial_t u = & D_1 \partial_{Q_a}^2 u + D_2 \partial_{T_a}^2 u - \partial_{Q_a} [f_1(Q_a, T_a, A_{\text{sys}}(t)) u] \\ & - \partial_{T_a} [f_2(Q_a, T_a, A_{\text{sys}}(t)) u] \end{aligned} \quad (\text{A10})$$

on the decade timescale with noise variances  $D_1 = 0.01$  and  $D_2 = 3$ , and Dirichlet boundary conditions on the domain  $(Q_a, T_a) \in [-0.04, 0.07] \times [295, 315]$  (so slightly larger than the physically realistic ranges). The paths  $A_{\text{sys}}(t)$  are chosen as described in Section III (equation (13)) and Section V (equation (22)) with  $A_{\text{sys}}^{\infty} = 0.47$  (the approximate present day value), and  $r$  and  $\epsilon$  varying such that we exceed the threshold  $A_{\text{sys}} = 0.5$  by time  $t_e^{(0.5)} \in [15, 40]$  years and amplitude  $R^{(0.5)} \in [0, 0.045]$ . For each simulation, we start from the eigenvector for the dominant (close to 1) eigenvalue of the Fokker-Planck operator on the right-hand side of (A10). The total simulation time period is chosen such that, after the transient time period,  $A_{\text{sys}}$  starts from close to its current day value, namely 0.471, and returns back to this value again at the end of the total simulation period. The escape probability is then calculated as

$$P_{\text{esc}}^{2d} = 1 - \int_{Q_a, T_a} u(Q_a, T_a, t_{\text{end}}) dQ_a dT_a, \quad (\text{A11})$$

at the end of an overall integration period (neglecting the escape during the transient time period). The resulting escape probabilities are shown in Figure 8a. The one-dimensional projection of the monsoon model (4) is extracted from the observable temperature  $T$ , using a second-order approximation of the known equilibrium curve  $(Q_a, T_a, A_{\text{sys}})$  and the attraction rate toward stable equilibria nearby. In practice, these quantities may have to be estimated from observations or model outputs. Then we use a modification of (A8), replacing the parabolic parameter path with the (rescaled) forcing of

the planetary albedo (22):

$$\dot{x} = D^{-2/3} a_0^2 \kappa (A_{\text{sys}}(D^{-1/3} t) - A_{\text{sys}}^b) + x^2. \quad (\text{A12})$$

In Eq. (A12) the parameter path  $A_{\text{sys}}(t)$  is given by (22),  $D = \mathbf{w}_0^T \text{diag}(0.01, 3) \mathbf{w}_0 = 3.04$  with  $\mathbf{w}_0 = (-3.50, -0.99)^T$ ,  $A_{\text{sys}}^b \approx 0.5287$ ,  $\kappa \approx 6 \cdot 10^{-3}$  and  $a_0 \approx$

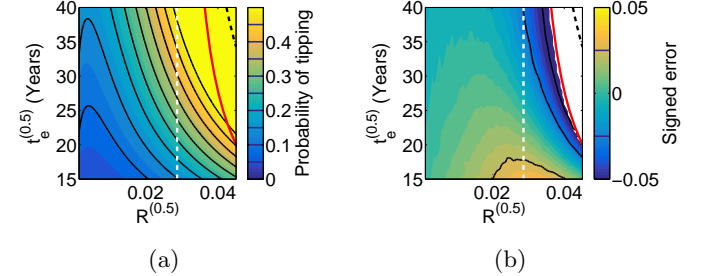


FIG. 8: Comparison between the escape probability as computed from the full two-dimensional model to its projection and approximation (20). (a) Escape probability  $P_{\text{esc}}^{2d}$ , as computed using (A10) and (A11). (b) Probability error of the mode approximation depicted in Figure 4 calculated as  $P_{\text{esc}}^{1d} - P_{\text{esc}}^{2d}$ . As in Figure 4, white dashed lines indicates the fold bifurcation, black dashed curve the critical parameter values for deterministic tipping and the red solid curve indicates the boundary for validity of the mode approximation.

115.30 ( $a_0^2 \kappa$  was estimated from decay rate and equilibrium curve of the 2d monsoon model).

The difference between the true escape rate and the mode approximation for the one-dimensional projected system (shown in Figure 8b) is less than 0.05 in absolute value everywhere in the region. The main source of error is that, due to the large noise variance, the system visits parts of the phase space where the quadratic approximation to the fold and the projection onto a single dimension are not accurate (the time scale separation between the two dimensions is only large close to the fold).

## Appendix B: Monsoon parameters and fitting coefficients

Section III discussed a simplification to the Indian Summer Monsoon model used by Zickfeld [11], though retaining the key dynamics behind the mechanisms of the monsoon. Table I lists all the parameters and their values used in the simplified monsoon model. The values of the fitting coefficients for the approximations of tipping probability  $P_{\text{esc}}$  are listed in Table II.

[1] T. M. Lenton, H. Held, E. Kriegler, J. W. Hall, W. Lucht, S. Rahmstorf, and H. J. Schellnhuber, Proceedings of the

National Academy of Sciences **105**, 1786 (2008).

TABLE I: Table of parameters used in Indian Summer Monsoon model

Parameter	Value	Unit
$T_{oc}$	300	$K$
$T_0$	273.2	$K$
$Q_{oc}$	0.0190	1
$Q_{sat}$	0.0401	1
$\mathcal{L}$	$2.5 \times 10^6$	$m^2 s^{-2}$
$C_E$	$3.4375 \times 10^{-4}$	$mm s^{-1} K^{-1}$
$C_P$	0.0027	$mm s^{-1}$
$C_{mo}$	$6.9021 \times 10^{-4}$	$mm s^{-1} K^{-1}$
$C_{ml}$	$1.6213 \times 10^{-4}$	$mm s^{-1} K^{-1}$
$C_{L1}$	1.6642	$Kg s^{-3} K^{-1}$
$C_{L2}$	-263.3753	$Kg s^{-3}$
$F_{\downarrow}^{SL,TA}$	443.6250	$Kg s^{-3}$
$C_H$	0.7136	$Kg s^{-3} K^{-2}$
$\theta_{oc}$	300.2356	$K$
$\Gamma_0$	0.0053	$K m^{-1}$
$\Gamma_1$	$5.5 \times 10^{-5}$	$m^{-1}$
$\Gamma_2$	1000	1
$\Gamma_a$	0.0098	$K m^{-1}$
$z_h$	$5.1564 \times 10^3$	$m$
$I_q$	$2.0636 \times 10^3$	$mm$
$I_T$	$1.1958 \times 10^9$	$Kg s^{-2} K^{-1}$
$\beta$	$3.1710 \times 10^{-9}$	$decades s^{-1}$

TABLE II: Table of fitting coefficients

Expression	coefficient	Value
Eq. (A1)	$c_0$	0.98
	$c_1$	(1.41, -0.97)
	$c_2$	(-0.22, -0.28, 0.33)
	$c_3$	(0.01, 0.03, 0.04, -0.04)
$\log \lambda_0(s) = \sum_{k=0}^3 c_k s^k$	$c$	(-1.3433, 1.3659,
in Eq. (A3)		-0.2347, 0.0277)
$\log \gamma_{1,4}(\bar{x}) = \sum_{k=0}^4 c_k \bar{x}^k$	$c$	(-1.0388, 0.0058,
in Eq. (A9)		-1.1687, -0.0409,
		-0.3326)

[2] H. Held and T. Kleinen, Geophysical Research Letters **31** (2004).

[3] M. M. Holland, C. M. Bitz, and B. Tremblay, Geophysical Research Letters **33** (2006).

[4] C. A. Boulton, L. C. Allison, and T. M. Lenton, Nature Communications **5** (2014).

[5] W. F. Laurance, B. Dell, S. M. Turton, M. J. Lawes, L. B. Hutley, H. McCallum, P. Dale, M. Bird, G. Hardy, G. Prideaux, *et al.*, Biological Conservation **144**, 1472

(2011).

[6] G. F. Clark, J. S. Stark, E. L. Johnston, J. W. Runcie, P. M. Goldsworthy, B. Raymond, and M. J. Riddle, Global Change Biology **19**, 3749 (2013).

[7] K. Siteur, E. Siero, M. B. Eppinga, J. D. Rademacher, A. Doelman, and M. Rietkerk, Ecological Complexity **20**, 81 (2014).

[8] P. Gandhi, E. Knobloch, and C. Beaume, Physical review letters **114**, 034102 (2015).

[9] W. Yan, R. Woodard, and D. Sornette, Physics Procedia **3**, 1641 (2010).

[10] P. Ashwin, C. Perryman, and S. Wieczorek, Nonlinearity **30**, 2185 (2017).

[11] K. Zickfeld, *Modeling large-scale singular climate events for integrated assessment*, Ph.D. thesis, Universitätsbibliothek (2004).

[12] A. Levermann, J. Schewe, V. Petoukhov, and H. Held, Proceedings of the National Academy of Sciences **106**, 20572 (2009).

[13] K. Zickfeld, B. Knopf, V. Petoukhov, and H. Schellnhuber, Geophysical Research Letters **32** (2005).

[14] N. Berglund and B. Gentz, *Noise-induced phenomena in slow-fast dynamical systems: a sample-paths approach* (Springer Science & Business Media, 2006).

[15] A. Majumdar, J. Ockendon, P. Howell, and E. Surovyanatkina, Physical Review E **88**, 022501 (2013).

[16] T. M. Lenton, Nature Climate Change **1**, 201 (2011).

[17] E. Hawkins, R. S. Smith, L. C. Allison, J. M. Gregory, T. J. Woollings, H. Pohlmann, and B. De Cuevas, Geophysical Research Letters **38** (2011).

[18] J. Zhu, Z. Liu, J. Zhang, and W. Liu, Climate Dynamics **44**, 3449 (2015).

[19] X. Li, S.-P. Xie, S. T. Gille, and C. Yoo, Nature Climate Change **6**, 275 (2016).

[20] P. D. Ditlevsen and S. J. Johnsen, Geophysical Research Letters **37** (2010).

[21] M. Scheffer, J. Bascompte, W. A. Brock, V. Brovkin, S. R. Carpenter, V. Dakos, H. Held, E. H. Van Nes, M. Rietkerk, and G. Sugihara, Nature **461**, 53 (2009).

[22] V. Dakos, M. Scheffer, E. H. van Nes, V. Brovkin, V. Petoukhov, and H. Held, Proceedings of the National Academy of Sciences **105**, 14308 (2008).

[23] M. Scheffer, S. R. Carpenter, T. M. Lenton, J. Bascompte, W. Brock, V. Dakos, J. Van De Koppel, I. A. Van De Leemput, S. A. Levin, E. H. Van Nes, *et al.*, science **338**, 344 (2012).

[24] P. Ritchie and J. Sieber, Chaos **26**, 093116 (2016).

[25] Y. A. Kuznetsov, *Elements of Applied Bifurcation Theory*, 3rd ed., Applied Mathematical Sciences, Vol. 112 (Springer-Verlag, New York, 2004) pp. xxii+631.

[26] C. Kuehn, *Multiple Time Scale Dynamics* (Springer, 2015).

[27] A. Neishtadt, Differential Equations **23**, 1385 (1987).

[28] A. Neishtadt, Differential Equations **24**, 171 (1988).

[29] C. Baesens, Physica D: Nonlinear Phenomena **53**, 319 (1991).

[30] S. M. Baer, T. Erneux, and J. Rinzel, SIAM Journal on Applied mathematics **49**, 55 (1989).

[31] T. Lenton, V. Livina, V. Dakos, E. Van Nes, and M. Scheffer, Philosophical Transactions of the Royal Society of London A: Mathematical, Physical and Engineering Sciences **370**, 1185 (2012).

[32] T. O’Riordan and T. Lenton, *Addressing tipping points for a precarious future* (Oxford University Press, 2013).

- [33] G. S. Bhat, *Quarterly Journal of the Royal Meteorological Society* **132**, 2583 (2006).
- [34] B. G. Liepert and A. Giannini, *Bulletin of the Atomic Scientists* **71**, 23 (2015).
- [35] V. Ramanathan, C. Chung, D. Kim, T. Bettge, L. Buja, J. Kiehl, W. Washington, Q. Fu, D. Sikka, and M. Wild, *Proceedings of the National Academy of Sciences of the United States of America* **102**, 5326 (2005).
- [36] M. Auffhammer, V. Ramanathan, and J. R. Vincent, *Proceedings of the National Academy of Sciences* **103**, 19668 (2006).
- [37] G. A. Meehl, J. M. Arblaster, and W. D. Collins, *Journal of Climate* **21**, 2869 (2008).
- [38] B. Knopf, M. Flechsig, and K. Zickfeld, *Nonlinear Processes in Geophysics* **13**, 531 (2006).
- [39] D. J. Seidel, G. Feingold, A. R. Jacobson, and N. Loeb, *Nature climate change* **4**, 93 (2014).
- [40] T. A. Driscoll, N. Hale, and L. N. Trefethen, *Chebfun guide* (Pafnuty Publications, Oxford, <http://www.chebfun.org/>, 2014).
- [41] P. Ritchie and J. Sieber, *Phys. Rev. E* **95**, 052209 (2017).